https://doi.org/10.5194/egusphere-2026-5207
Preprint. Discussion started: 11 September 2026

Reconciling online and offline source apportionment of brown carbon absorption in wintertime Seoul

Hwajin Kim[1,2,*] and Yanfang Chen[2,3]

1 Department of Environmental Health Sciences, Graduate School of Public Health, Seoul National University, Seoul 08826, Republic of Korea

2 Institute of Health and Environment, Seoul National University, Seoul 08826, Republic of Korea

3 Now at Paul Scherrer Institute (PSI), Villigen, Switzerland

** Correspondence: Hwajin Kim (khj0116@snu.ac.kr)*

Abstract

Brown carbon (BrC) is a leading uncertainty in aerosol radiative forcing, and the source-resolved mass absorption coefficients (MAC) used in climate models come from both real-time (online) and filter-based (offline) measurements. Both are widely trusted, yet have rarely been applied to the same aerosol and compared source by source, leaving the assumption that they are interchangeable untested. Here we ask whether online and offline source apportionment yield the same sources of BrC absorption for wintertime urban aerosol. We combined a seven-wavelength aethalometer with high-resolution aerosol mass spectrometry (online, whole particle) and 24 h PM2.5 filter UV–Vis of water extracts (offline), attributing bulk absorption to positive-matrix-factorization factors by regression on each platform. The two platforms agreed on the bulk attribution (winter BrC carried by secondary and biomass-burning OA) and on consistency with worldwide observations, but inverted the source ranking: online, biomass burning and less oxidized secondary organic aerosol dominated while more oxidized OA (MO-OOA) was negligible (MAC 0.07 $m^2 g^{-1}$); offline, MO-OOA dominated (0.88 $m^2 g^{-1}$). This reversal reflects how the sample is measured, not an atmospheric change: water-soluble selection and a likely shift of MO-OOA toward reduced-nitrogen chromophores during offline preparation, while bulk composition and factor time series are preserved. The source inferred for BrC absorption is therefore strongly dependent on method and integration time, a critical caution for source-resolved BrC parameterizations that treat online and offline datasets as interchangeable.

https://doi.org/10.5194/egusphere-2026-5207
Preprint. Discussion started: 11 September 2026

1 Introduction

Organic aerosol (OA) constitutes a large fraction of fine particulate matter ($PM_{2.5}$) and influences the Earth's radiative budget through the scattering and absorption of solar radiation. While OA was historically treated as purely scattering, the recognition of a light-absorbing fraction, "brown carbon" (BrC), has required a revision of how organics are represented in climate models (Andreae and Gelencsér, 2006; Laskin et al., 2015, 2025). BrC absorbs efficiently in the near-ultraviolet (UV) and short visible wavelengths and is distinguished from black carbon (BC) by a much steeper wavelength dependence, i.e. a larger absorption Ångström exponent (AAE). Model estimates place the direct radiative forcing of BrC at ~+0.22 to +0.58 W m^{-2}, equivalent to ~25–70 % of BC absorption and, in biomass-burning regions, up to ~60 % (IPCC, 2013; Saleh et al., 2014). The wide spread across these estimates, which persists in recent observation-constrained and Earth-system-model assessments (Cheng et al., 2024; DeLessio et al., 2024), makes BrC one of the leading uncertainties in the aerosol forcing budget.

The sources of BrC are diverse. Primary BrC is emitted directly by incomplete combustion, biomass burning, residential heating and traffic, with the chromophore content set by fuel and burning conditions (Saleh et al., 2014). Secondary BrC forms through gas- and aqueous-phase oxidation of biogenic, anthropogenic and combustion-derived volatile organic compounds, with the yield of light-absorbing products governed by precursor type, oxidant regime and particle acidity (Laskin et al., 2015, 2025). Both channels are active in urban winter atmospheres, where combustion emissions coexist with photochemical and nocturnal aqueous processing.

A central uncertainty concerns how BrC absorption evolves after emission. Online, in-situ measurements frequently show "photobleaching", in which exposure to sunlight and oxidants fragments chromophores and rapidly reduces absorptivity (Zhao et al., 2015; Wong et al., 2019; Hems and Abbatt, 2018), with reported bleaching half-lives of order ~9–15 h that are strongly source-dependent (Qiu et al., 2026) and regional first-order rates near ~0.2–0.24 day^{-1} in East and South Asian outflow (Dasari et al., 2019; Fang et al., 2023). Other studies, particularly those involving aqueous-phase chemistry or high-NO_x conditions, report "browning", in which aging generates new, stable chromophores such as nitro-aromatics and imidazole derivatives (Laskin et al., 2015; Zhang et al., 2016). Increases in the oxygen-to-carbon (O/C) ratio have been correlated with both loss and gain of absorption in different datasets (Li et al., 2023), so the sign of the O/C–absorption relationship is not universal, a fact we show is partly an artifact of how the absorption is measured.

https://doi.org/10.5194/egusphere-2026-5207
Preprint. Discussion started: 11 September 2026

This apparent contradiction is exacerbated by the measurement approach. Online methods (multi-wavelength aethalometers combined with aerosol mass spectrometry) capture the rapid diurnal variation and the net optical state of the suspended particle. Offline, filter-based methods provide detailed chemical speciation of solvent-extractable fractions but integrate over long periods (typically 24 h), potentially conflating day and night chemistry and introducing extraction- or drying-related artifacts. A growing body of work now couples the two, for example by regressing filter-based UV–Vis absorption onto PMF factors to obtain source-resolved water-soluble MAC (Moschos et al., 2018), and by constraining source-resolved absorption from online aethalometer and speciation data (Navarro-Barboza et al., 2025; Rovira et al., 2026), and several studies have folded source-resolved MAC and photobleaching rates directly into models (Fang et al., 2023). Reconciling online and offline results is therefore not a technical detail but a prerequisite for the source-resolved BrC parameterizations these models require. Yet, to our knowledge, the two approaches have not previously been applied to the same aerosol and compared at the level of individual sources; where prior coupling studies report agreement, they compare like with like (same solubility class or same instrument stream), leaving the cross-phase comparison a modeler implicitly makes untested.

Seoul offers a well-suited testbed for this reconciliation. Seoul is a year-round BrC absorber whose signal is strongest and most stable in winter, the season targeted here (Kim et al., 2016), when the East Asian heating season injects a large pulse of biomass-burning and fossil-fuel combustion emissions rich in aromatic precursors (phenols, methoxyphenols, polycyclic aromatic hydrocarbons) and co-emitted with high concentrations of nitrogen oxides. The source mix is intermediate between the secondary-dominated regime typical of many Asian sites and the biomass-burning-dominated regime of Europe and North America (Kasthuriarachchi et al., 2020), providing a stringent test of source-resolved attribution. In this study we (i) quantify the factor-resolved contribution of OA sources to BrC absorption using online measurements; (ii) apply the same attribution to the offline water-soluble fraction; and (iii) reconcile the resulting online–offline discrepancy, identifying what actually controls the source inferred for BrC absorption. The central result, that the two platforms agree on the bulk BrC burden and with the literature, but invert the source ranking, and that the reversal is governed by the measurement window rather than by the aerosol, has direct consequences for how source-resolved BrC is represented in models.

2 Materials and methods

2.1 Sampling site and campaign

The field campaign was conducted in the 2018 winter campaign (23 October – 4 December 2018) at the Korea Institute of Science and Technology (KIST) in the Seongbuk district of northeastern Seoul (37.60° N, 127.05° E). The site lies ~7 km from the dense city center and represents a typical urban-background

https://doi.org/10.5194/egusphere-2026-5207
Preprint. Discussion started: 11 September 2026

environment; the sampling inlet was on the rooftop of a campus building, ~60 m above sea level, within the urban canopy layer but away from the immediate influence of street canyons. The location is affected by a diverse mix of local sources, vehicular exhaust from nearby roads and a major arterial highway (~400 m), residential heating and localized biomass burning from surrounding high-density housing, and is periodically influenced by the long-range transport of aged continental air masses, most frequently during northwesterly winter flow.

2.2 Online measurements

Real-time chemical composition of non-refractory PM_1 was measured with an Aerodyne high-resolution time-of-flight aerosol mass spectrometer (HR-ToF-AMS; DeCarlo et al., 2006). Elemental ratios (O/C, H/C) were computed with the "Improved-Ambient" method (Canagaratna et al., 2015). Aerosol light absorption was measured at seven wavelengths (370, 470, 520, 590, 660, 880 and 950 nm) with a dual-spot aethalometer (AE33, Magee Scientific), which compensates for the filter-loading effect in real time (Hansen et al., 1984; Drinovec et al., 2015). The absorption coefficient attributable to BrC ($b_{abs,BrC}$) at 370 nm was obtained by subtracting the BC contribution, assuming a BC AAE of 1.0. Because this AAE-subtraction estimate is sensitive to the chosen reference wavelength and to the assumed AAE_{BC} (Navarro-Barboza et al., 2025), we test its robustness in the Supplement (Table S4). Importantly, while varying the assumed AAE_{BC} alters the absolute BrC absorption fraction, the resulting change is systematic across the campaign and does not affect the relative source ranking derived from the PMF-regression analysis, ensuring the robustness of our core findings.

2.3 Offline measurements

$PM_{2.5}$ samples were collected on pre-baked quartz-fiber filters using a high-volume sampler with a 24 h integration time. Water-soluble organic carbon (WSOC) was extracted by ultrasonication in deionized water. Absorption spectra of the extracts were measured with a UV–Vis spectrophotometer (Cary 5000, Varian). The mass absorption efficiency (MAE) of the extracted BrC was calculated by normalizing the water-soluble BrC absorption coefficient at 365 nm ($b_{abs,WS\text{-}BrC}$) by the corresponding (WSOC or total OA) mass concentration, following the earlier Seoul record (Kim et al., 2016) to enable direct comparison.

To obtain the water-soluble OA composition in the same fragment space as the online AMS, the 24 h $PM_{2.5}$ quartz-filter samples were analyzed by offline aerosol mass spectrometry (offline-AMS) following the established protocol of Daellenbach et al. (2016) and its argon implementation by Bozzetti et al. (2017); the full extraction, nebulisation and blank-correction details are given in the Supplement (Sect. S1.2, Table S1). Briefly, a water extract of each filter was atomised in argon, dried, and sampled by the same HR-ToF-

https://doi.org/10.5194/egusphere-2026-5207
Preprint. Discussion started: 11 September 2026

AMS (vaporiser 600 °C) used for the online measurements, with the NH_4NO_3 interference on the CO_2^+ signal corrected following Pieber et al. (2016) and elemental ratios derived by the Improved-Ambient method (Canagaratna et al., 2015). Because offline-AMS resolves the water-soluble OA composition but not its absolute mass, the total water-soluble organic aerosol mass of each sample was quantified as WSOA = WSOC × (OM:OC), with WSOC measured on the same filter by a TOC analyzer and OM:OC obtained from the offline-AMS elemental analysis; each PMF factor was then placed on an atmospheric water-soluble mass basis by scaling this total WSOA by its fractional contribution to the offline organic signal (Table S1). This yields, for each 24 h sample, a source-resolved offline factor time series directly comparable with the online record (Sect. 2.4). The two datasets are consistent at the bulk level: 24 h-averaged online PM_1 OC and OA track the co-located offline $PM_{2.5}$ filter values with regression slopes of 0.85 and 0.86 (r^2 = 0.88 and 0.89), the small deficits being consistent with the PM_1 versus $PM_{2.5}$ size cut. The absorption comparison, by contrast, separates the two solvents: the online 370 nm BrC absorption follows the methanol-soluble offline absorption (slope 0.72, r^2 = 0.70) but not the water-soluble absorption (r^2 = 0.25; Fig. S4). The two platforms therefore sample the same aerosol mass, and the online–offline differences developed in Sect. 3.3 originate in the water extract, which recovers only the water-soluble part of the absorbing material.

2.4 Source apportionment and online–offline factor correspondence

Positive matrix factorization (PMF; Paatero and Tapper, 1994), implemented with the PMF2 algorithm following the AMS factor-analysis procedures established (Ulbrich et al., 2009; Zhang et al., 2011a), was applied independently to the online and to the offline organic high-resolution mass-spectral matrices. The online solution, applied to the time-resolved AMS spectra, resolved six OA factors: three primary, hydrocarbon-like OA (HOA), cooking OA (COA) and biomass-burning OA (BBOA), and three secondary, two less-oxidized oxygenated OA factors (LO-OOA1, LO-OOA2) and one more-oxidized oxygenated OA factor (MO-OOA); the high-resolution mass spectra of all six online factors are shown in Fig. S1b, and their source-resolved optical roles are developed in Sect. 3.2 (Fig. 2). The diagnostics supporting the six-factor choice, and the comparison with the neighboring five- and seven-factor solutions, are given in the Supplement (Figs. S1, S2).

The offline solution was obtained from a separate, unconstrained PMF on the offline-AMS matrix, one water-soluble high-resolution mass spectrum per 24 h filter, with no online factor profiles imposed as *a priori* information, resolving four water-soluble factors (a combined primary/POA factor, BBOA, LO-OOA and MO-OOA). Four factors is the smallest solution in which every factor is separately interpretable and finds an independent counterpart in the online apportionment; the comparison with the neighboring three-

https://doi.org/10.5194/egusphere-2026-5207
Preprint. Discussion started: 11 September 2026

and five-factor solutions is given in the Supplement (Fig. S3; Sect. S1.3). Their water-soluble high-resolution mass spectra are shown in Fig. S3b, and the optical consequences of this solution are developed in Sect. 3.3 (Fig. 7).

Because the two solutions are independent, the correspondence between an online and an offline factor is established *a posteriori* rather than imposed: each offline factor was matched to its online counterpart by the similarity of its high-resolution mass spectrum (pairwise spectral R^2 in Table S2) and by the correlation of its concentration time series with the 24 h-averaged online factor over the paired filter days (Fig. S8). The four offline factors map onto the six online factors, the online HOA and COA factors combining into the single offline primary/POA factor; for MO-OOA, the factor central to the online–offline comparison, the two time series correlate at r = 0.93. The residual fragment-level differences between the matched spectra (Fig. 9) are therefore not evidence of a different factor; they quantify the preparation-induced chemical shift of Sect. 3.3. Each offline factor was additionally checked against measurements not used in the apportionment: levoglucosan and K^+ for BBOA, EC for the primary/POA factor, and WSOC and sulfate for the oxygenated factors (Table S2).

2.5 Attribution of absorption to OA sources

Following the widely used regression approach (Moschos et al., 2018), the bulk BrC absorption coefficient was attributed to individual OA factors by origin-forced multiple linear regression (MLR) of the measured absorption coefficient onto the PMF factor mass time series:

$$b_{abs,BrC}(\lambda) = \sum_{i=1}^{n} MAC_i(\lambda) m_i + \varepsilon \qquad (1)$$

where m_i is the mass concentration of OA factor i, $MAC_i(\lambda)$ is its mass absorption coefficient at wavelength λ, n is the number of factors and ε is the residual; the regression is forced through the origin, so that the coefficient retrieved for each factor is directly its MAC. The identical regression was applied to the online ($b_{abs,BrC}$ at 370 nm) and offline ($b_{abs,WS\text{-}BrC}$ at 365 nm) datasets, so that any difference in the resulting source ranking reflects the measurement platform rather than the attribution method. Regression uncertainties, collinearity diagnostics and a non-negative least-squares sensitivity test are reported below and in the Supplement (Table S3).

MLR of absorption onto co-varying factor time series can be affected by collinearity, which inflates coefficient uncertainties and can produce unphysical negative coefficients. We therefore report the condition number of the factor matrix, the variance-inflation factor of each factor and bootstrap 95 % confidence intervals on every MAC, and cross-check both fits with a non-negative least-squares refit; the full diagnostics and interval estimates are given in the Supplement (Table S3).

https://doi.org/10.5194/egusphere-2026-5207
Preprint. Discussion started: 11 September 2026

3 Results and discussion

3.1 Bulk optical properties: ubiquitous, secondary-influenced BrC

The campaign-averaged aethalometer spectra showed the wavelength dependence characteristic of mixed carbonaceous aerosol, with the absorption coefficient decreasing steeply toward longer wavelengths (Fig. 1a). Because pure BC has an AAE near 1.0 and absorption at 880–950 nm is BC-dominated by definition, the excess absorption in the UV and blue could not be explained by BC alone: the contribution of BrC to absorption at 370 nm reached ~25 % (Fig. 1a), demonstrating the ubiquitous presence of light-absorbing organics beyond BC. The median AAE of the BrC fraction was ~5, confirming that the organic absorption is strongly concentrated in the UV and short-visible wavelengths, as expected for brown rather than black carbon (AAE ~1; Fig. 1b).

3.2 OA sources and their optical roles

The OA sources were dominated by secondary OA. The two LO-OOA factors and MO-OOA together made up the large majority of the OA mass, with MO-OOA showing an aged signature (O/C ~0.90) and a midday photochemical maximum correlated with odd oxygen ($O_x = O_3 + NO_2$), while the LO-OOA factors had lower O/C (~0.64) and distinct diurnal behavior, one peaking at night (LO-OOA2) and one comparatively flat through the day (LO-OOA1). Primary factors (HOA, COA, BBOA) were a minor mass fraction. On average, secondary OA accounted for > 60 % of the BrC absorption.

Attributing the 370 nm BrC absorption to these factors by MLR gave a clear ranking (Table 1; Fig. 2). BBOA was the single most efficient absorber (MAC ~5.7 $m^2\ g^{-1}$), followed by the two less-oxidized secondary factors (LO-OOA1 ~4.2 and LO-OOA2 ~3.0 $m^2\ g^{-1}$); HOA was weakly absorbing (~0.65 $m^2\ g^{-1}$), COA negligible, and MO-OOA effectively non-absorbing (~0.07 $m^2\ g^{-1}$). In terms of the share of BrC absorption at 370 nm, the LO-OOA factors together contributed ~68 %, BBOA ~26 %, and HOA ~6 %. This split places Seoul between the two typical urban regimes seen across other source-apportioned datasets (Table 2).

Table 2 places the Seoul attribution against other urban sites on a common absorption basis: for the compiled single-site studies, each study's OA-factor mass fractions are weighted by this study's measured factor MACs (Table 1) and normalized, so every row is a contribution to BrC absorption rather than to OA mass. Read this way, the sites separate not by continent but by season. The most strongly secondary-dominated sites are the non-winter ones — Shanghai in late spring (~93 %), Hong Kong (~91 %), the summertime rural southeastern US (~68 %) and tropical Singapore (~58 %) — where sustained photochemical and aqueous processing builds a large less-oxidized secondary absorber pool and biomass

https://doi.org/10.5194/egusphere-2026-5207
Preprint. Discussion started: 11 September 2026

burning is minor or absent. The wintertime, mid- to high-latitude sites, by contrast, all carry a large combustion contribution: coal- and wood-burning Lanzhou (~66 %), the European winter cities Barcelona, Paris and Helsinki (~35–49 %), and above all the season-matched Chinese megacities of Wang et al. (2022), where primary combustion dominates and secondary formation contributes only ~7 % in the north and ~18–21 % in the south — consistent with an independent ^{14}C apportionment that assigns two-thirds of Beijing's light-absorbing carbon to fossil, coal-dominated combustion (Yan et al., 2017). Seoul is the exception among the winter sites: it shares their combustion signature (~26 %, the shared winter-heating tail of high-latitude East Asia) yet remains far more secondary (~68 %) than any other wintertime city in the table. The apparent "Asian-secondary versus European-biomass-burning" split of earlier compilations is therefore largely a seasonal artifact — the secondary-dominated Asian sites are simply the non-winter ones — and the genuinely transferable result from Seoul is its co-dominance, unusual for winter, of a strong less-oxidized secondary pool with a biomass-burning source. It is that secondary contribution — under-represented both by the biomass-burning-dominated winter literature and by single bulk-OOA parameterizations — that is the meaningful and generalizable finding.

The absolute factor MAC values are likewise consistent with the literature (Fig. 2). BBOA (~5.7 $m^2\ g^{-1}$) lies at the upper end of the pan-European residential-combustion range, close to the residential-coal (CCOA ~4.66) and wood-burning (~3.52) values reported for the pan-European dataset (Rovira et al., 2026), and within the fresh biomass-burning range (2.1–5.7 $m^2\ g^{-1}$; Yang et al., 2025). The less-oxidized secondary factors (LO-OOA1 ~4.2, LO-OOA2 ~3.0) lie well above the near-zero MAC (~0–1) typical of bulk oxidized OA but match strongly-absorbing secondary/"night-time" BrC reported elsewhere ("Night-OA" ~2.3; Kuang et al., 2025, Pearl River Delta), and HOA (~0.7) is within the literature range. That the resolved factors fall within independently-reported ranges confirms they are physically reasonable absorbers rather than regression artifacts. This agreement with independent datasets suggests that these per-source absorptivities are transferable rather than unique to this campaign.

3.2.1 Biomass burning is the most efficient absorber and the principal nitrogen source

Biomass burning is the most efficient absorber the regression resolves. BBOA carries a MAC of 5.66 $m^2\ g^{-1}$ (Table 1), above both less-oxidized secondary factors (4.22 and 2.94 $m^2\ g^{-1}$) and nearly two orders of magnitude above MO-OOA (0.07 $m^2\ g^{-1}$); the factor matrix is well conditioned and the bootstrap 95 % confidence intervals separate every online factor from zero (Table S3), so this ranking is statistically robust. Its optical weight is visible in the raw record before any regression: $b_{abs,BrC}$ at 370 nm tracks the BBOA mass excursions episode by episode, and the largest absorption peaks of the campaign coincide with the biomass-burning plumes (Fig. 3a). Sorting the record by the BBOA mass fraction makes the dependence monotonic, binned median $b_{abs,BrC}$(370 nm) rises from ~8 Mm^{-1} when BBOA is below 2 % of OA to ~27

https://doi.org/10.5194/egusphere-2026-5207
Preprint. Discussion started: 11 September 2026

Mm^{-1} in the 12–15 % bin (Fig. 3b), so a source that is a minor mass contributor in wintertime Seoul nevertheless sets the upper envelope of the observed absorption and supplies ~26 % of it.

This optical weight comes with a distinct nitrogen signature. BBOA is the most nitrogen-rich factor of the campaign (N/C = 0.053, against 0.012 for LO-OOA1), with $C_xH_yN^+$ and $C_xH_yNO_z^+$ fragments spread across the whole spectrum rather than confined to a few marker ions (Fig. 3c). The ambient record shows the same coupling: at a given biomass-burning fraction the most absorbing points carry the largest CHN + CHON concentrations (color scale, Fig. 3b), and both nitrogen ion families gain mass fraction as BBOA/OA rises (Fig. 3d).

Possible chromophores fall into the two classes documented for biomass-burning aerosol: oxidized nitroaromatics (nitrophenols, nitrocatechols), detected as $C_xH_yNO_z^+$ ions, and reduced-nitrogen heterocycles (imidazoles, pyrazines), detected as $C_xH_yN^+$ ions (Laskin et al., 2015). Offline speciation of filters collected at this site over the same period confirms that a reduced-nitrogen pool is present: water-soluble aliphatic amines (mono-, di- and trimethylamine) were elevated in the winter samples and the free amino acids Gly, Ala and Thr tracked local combustion (Baek et al., 2022). Both can be emitted directly by burning — the amines from fuel nitrogen and the amino acids from the proteinaceous fraction of the biomass (Ge et al., 2011; Laskin et al., 2015) — consistent with the primary nitrogen enrichment resolved here for BBOA; part of the same pool can also form secondarily in aerosol water, a route taken up in Sect. 3.2.2.

As a fresh, weakly oxidized source (O/C = 0.37), biomass burning also emits the precursors of further nitrogen chromophores, carbonyls together with the ammonia and amines released from nitrogen-containing fuel, which react in aerosol water (Bones et al., 2010; Updyke et al., 2012). Since the less-oxidized secondary factors carry ~68 % of the 370 nm absorption against ~26 % for primary BBOA, that indirect route is likely the more consequential one for the nitrogen-associated secondary absorption, and the same nitrogen signature indeed reappears in the secondary pool without the biomass-burning markers (Sect. 3.2.2).

3.2.2 Nighttime secondary BrC is nitrogen-associated

The nitrogen signature is not confined to the primary plume. Among the secondary factors, whole-particle BrC absorption at 370 nm covaries with LO-OOA2 (r^2 = 0.45) but not with the daytime factor LO-OOA1 (r^2 = 0.10; Fig. 4a), and the two quantities share a diurnal shape — LO-OOA2 mass and $b_{abs,BrC}$(370 nm) both rise through the night and decay through the day, whereas the odd-oxygen-driven MO-OOA peaks at midday (Fig. 4c). The absorption associated with LO-OOA2 is therefore acquired at night, when photochemical SOA production is at a minimum.

https://doi.org/10.5194/egusphere-2026-5207
Preprint. Discussion started: 11 September 2026

In Fig. 4a the points are graded by their $C_xH_yN^+$ loading, and the highest absorption coincides with the most nitrogen-rich points: absorption and the nitrogen-containing fragments vary together within the factor rather than merely coexisting in it. The correlations confirm this ion by ion. LO-OOA2 and BBOA correlate positively with the $C_xH_yN^+$ fragments (r = 0.72, range 0.58–0.86, and r = 0.78, 0.65–0.90), whereas LO-OOA1 does not (r = −0.40; Fig. 4b). LO-OOA2 also tracks the secondary inorganic ions (NO_3^-, SO_4^{2-}, NH_4^+), as expected for a pool formed under humid, stagnant nocturnal conditions, while chloride, a primary combustion tracer, shows no correlation. Because the correlation extends across the whole $C_xH_yN^+$ series rather than resting on a few peaks, the absorption of LO-OOA2 is associated with the reduced-nitrogen organic pool as a whole, whereas the negative correlation for LO-OOA1 places its chromophores outside that pool (Sect. 3.2.3).

As in BBOA, this nitrogen sits predominantly in the reduced-nitrogen $C_xH_yN^+$ family rather than the oxidized $C_xH_yNO_z^+$ family, with fragments consistent with imidazole-type structures (Fig. S7). Carbonyl condensation with ammonium and amines in aerosol water is the pathway most consistent with that partitioning (Bones et al., 2010; Updyke et al., 2012; Laskin et al., 2015), consuming the biomass-burning precursors of Sect. 3.2.1 together with dicarbonyls from aromatic and biogenic VOC oxidation; identifying the individual heterocycles would require molecular-level speciation.

Nocturnal conditions favor that chemistry: a shallow boundary layer concentrates the precursors, high relative humidity sustains the aerosol liquid water in which the condensation proceeds, and the absence of sunlight suspends photobleaching. Nitrate-radical nitration of biomass-burning phenols may contribute as well, yielding strongly absorbing nitroaromatics (Iinuma et al., 2010; Rana and Guzman, 2022), although our measurements do not constrain its share. Light-absorbing nitrogen therefore accumulates overnight, and the secondary share of $b_{abs,BrC}$ is largest at night and smallest at the midday radiation maximum (Fig. 4c).

After sunrise, LO-OOA2 mass and $b_{abs,BrC}$(370 nm) decline together, mainly through dilution by the deepening boundary layer with no daytime source to replenish the pool — the same dynamics as the morning decline of primary BBOA — with oxidative conversion to the optically negligible MO-OOA superimposed (Sect. 3.2.3).

The optical footprint of biomass burning therefore extends beyond the primary BBOA factor, and the water-soluble nighttime pool it feeds — preserved on a 24 h filter but bleached in real time — is where the two platforms disagree (Sect. 3.3).

https://doi.org/10.5194/egusphere-2026-5207
Preprint. Discussion started: 11 September 2026

3.2.3 LO-OOA1 absorbs without nitrogen and bleaches by day

LO-OOA1 absorbs strongly (MAC ~4.2 $m^2\ g^{-1}$) yet is essentially nitrogen-free (N/C ~0.012): its mass spectrum is enriched in the non-nitrogenous aromatic fragments *m/z* 77 and 91 — established markers of aromatic ring structures — and shows no nitrate-related chromophore signature (Fig. 5). Its absorption therefore arises not from nitroaromatics but from non-nitrogenous aromatics, and this is quantitatively sufficient: strongly-conjugated aromatics can absorb at several times their carbon mass, so even a small aromatic mass fraction (< 5 %) can dominate a factor's absorption (Laskin et al., 2015; Yuan et al., 2020). This does not contradict the evidence that nitrogen-containing chromophores ('brown nitrogen') dominate organic-aerosol absorption in the aggregate (Li et al., 2025); rather, LO-OOA1 is a well-constrained field example of the non-nitrogenous aromatic pool that co-exists with, and is distinct from, the nitrogen-driven nighttime factors.

Despite being an efficient absorber, LO-OOA1 does not lead the ambient BrC absorption: its diurnal mass is nearly flat — a slight morning rise followed by a daytime decline (Fig. 4c; mean diurnal cycles of all secondary OA factors are compared in Fig. S6). Its continuous secondary production appears to be offset by rapid daytime photochemical loss, and the ambient absorption falls even though the absorbing factor does not: $b_{abs,BrC}$(370 nm) drops from ~18 Mm^{-1} before sunrise to ~11 Mm^{-1} in the early afternoon, in antiphase with incoming solar radiation, and the secondary share of that absorption is largest at night, when MO-OOA is at its minimum (Fig. 4c). Odd oxygen ($O_x = O_3 + NO_2$) rather than clock time shows the conversion directly: the daytime points grade with O_x, the highest LO-OOA1 fractions carrying the lowest O_x and the highest-O_x points falling to below 10 % LO-OOA1 while MO-OOA approaches 50 % of OA (color scale, Fig. 6), so the loss of the absorbing pool scales with photochemical processing and not merely with time of day. Between 09:00 and 16:00 LT the LO-OOA1 and MO-OOA fractional contributions are correspondingly anti-correlated (slope −0.78, r = −0.69; Fig. 6), tracing the photochemical conversion of the absorbing LO-OOA1 pool to the more-oxidized, non-absorbing MO-OOA: as solar radiation and oxidants (O_3, OH) rise through the day, the conjugated aromatic systems that carry LO-OOA1's absorption are progressively cleaved, raising the oxidation state and removing the chromophores (photobleaching; cf. Li et al., 2023).

MO-OOA completes the picture from the opposite end of the oxidation scale. It is the most oxidized factor resolved (O/C ~0.90) and the least absorbing (MAC 0.07 $m^2\ g^{-1}$), consistent with the expectation that the steps raising O/C — OH addition, ring opening and C–C fragmentation — also dismantle the extended conjugation on which near-UV absorption depends, converting aromatic rings and nitrogen heterocycles into smaller, more oxygenated and weakly absorbing products (Laskin et al., 2015; Li et al., 2023).

https://doi.org/10.5194/egusphere-2026-5207
Preprint. Discussion started: 11 September 2026

Oxidation state is therefore a poor optical predictor in this aerosol: absorption tracks chromophore structure — aromatic conjugation in LO-OOA1, reduced-nitrogen heterocycles in LO-OOA2 and BBOA — and is progressively lost as that structure is oxidized away. The whole-particle record carries the same signature, with online babs,BrC(370 nm) falling as O/C rises (Fig. 8) — a field measure of BrC whitening with daytime aging. Against this factor-level picture, the positive absorption–O/C slope of the offline record is unlikely to be a property of the airborne aerosol, and its origin is examined next (Sect. 3.3).

3.3 One evolving aerosol and the online–offline reversal

Sections 3.1–3.2 characterized the airborne aerosol through the online platform, which described a single diurnally evolving BrC: at night a shallow boundary layer and high humidity drive aqueous formation of nitrogen-containing chromophores in BBOA and LO-OOA2, while by day photochemistry converts LO-OOA1 to MO-OOA, O/C rises and absorption fades. The identical source-resolved attribution is next applied to the offline platform — the same aerosol, collected on 24 h $PM_{2.5}$ filters and measured as its water-soluble extract — to examine whether the same sources of BrC absorption are identified. At the bulk level the two records agree: the offline water-soluble MAE_{365} of this study (~1.3 $m^2\ gC^{-1}$) falls within the range of the water-soluble BrC literature and reproduces the earlier Seoul offline record (Kim et al., 2016; Fig. S9). The divergence emerges only when the attribution is source-resolved.

3.3.1 The two platforms invert the source ranking for the same aerosol

Taken in isolation, the offline platform yields an internally consistent attribution dominated by the most-oxidized secondary factor. In the water-soluble source-resolved regression, MO-OOA is by far the strongest absorber (0.88 $m^2\ g^{-1}$), the combined primary/POA term is weak (0.61 $m^2\ g^{-1}$), BBOA is small (0.64 $m^2\ g^{-1}$) and LO-OOA is statistically indistinguishable from zero (Fig. 7 and Table 1). The offline record alone would therefore indicate that wintertime Seoul BrC absorption is carried predominantly by aged, highly-oxidized secondary OA and — on the basis of the absorption–O/C relationship — that BrC absorption increases as the aerosol oxidizes (offline $b_{abs,WS\text{-}BrC}$(365 nm) increases with O/C; Fig. 8). This secondary-plus-biomass-burning attribution echoes the earlier Seoul offline record of Kim et al. (2016), whose water-soluble organic carbon correlated strongly with both levoglucosan (biomass burning) and dicarboxylic acids (secondary formation).

This conclusion is opposite to that obtained from the online platform for the same aerosol (Sect. 3.2). Online, BBOA (5.66 $m^2\ g^{-1}$) and the two less-oxidized secondary factors (4.22 and 2.94 $m^2\ g^{-1}$) dominate the absorption while MO-OOA is essentially non-absorbing (0.07 $m^2\ g^{-1}$), and $b_{abs,BrC}$(370 nm) decreases with O/C (photobleaching). The source ranking thus inverts completely between the two platforms (Table 1; Fig. 7) and even the sign of the absorption–O/C relationship flips (Fig. 8). Crucially, this disagreement is

https://doi.org/10.5194/egusphere-2026-5207
Preprint. Discussion started: 11 September 2026

confined to the source level: the two platforms agree on the bulk aerosol. The online mass absorption efficiency (~3.5 $m^2 g^{-1}$, total-OA basis) is consistent with our offline record, with the earlier Seoul offline record (Kim et al., 2016) and with the water-soluble BrC literature (Moschos et al., 2021; Zhang et al., 2011b; Tang et al., 2021; Fig. S9), all of which attribute wintertime absorption to a mixture of secondary and biomass-burning OA; the absolute online–offline MAE gap is itself an expression of the water-soluble cut examined below (whole-particle total-OA basis online versus water-soluble-carbon basis offline; Fig. S9 caption), not an inconsistency. The discrepancy is therefore well defined and diagnostic: the two measurement windows agree on the amount of BrC present and on its bulk attribution, yet invert the source to which it is attributed.

3.3.2 The reversal decomposes into solubility selection and preparation-induced browning

The reversal does not indicate that either platform is erroneous; it follows directly from what each platform samples and, crucially, from a chemical change that the offline preparation itself most plausibly introduces — the formation of new light-absorbing reduced-nitrogen chromophores during extraction, atomization and drying (e.g., Nguyen et al., 2012; Updyke et al., 2012). Two mechanisms may account for the reversal: solubility selection, which removes the water-insoluble strong absorbers from the offline window, and preparation-induced browning, which makes the most water-soluble factor absorb in the extract.

First, solubility selection: the offline UV–Vis sees only the water-soluble OA, and this pool is systematically more oxidized. The whole-particle 370 nm absorption tracks the methanol-soluble offline absorption far more closely than the water-soluble fraction (Fig. S4), so a substantial part of the absorbing material is not water-extractable, whereas MO-OOA is recovered almost quantitatively in the extract (Fig. S5), its offline factor time series following the online factor (Fig. S8). For BBOA and LO-OOA the strong chromophores (nitro-aromatics, PAHs, quinones) are known to be largely water-insoluble, so far less of their absorption than of their mass survives extraction and their apparent MAC collapses — the online-dominant absorbers largely vanish from the offline attribution. Selection alone, however, cannot brown MO-OOA. The extract retains the oxidized, predominantly colorless fragments ($C_xH_yO^+$ and CO_2^+ at offline/online ratios of 1.0-1.2) while stripping the hydrocarbon fragments ($C_xH_y^+$ to 0.54), so a purely selected pool should remain optically weak — yet the offline MO-OOA is the strongest water-soluble absorber.

Second, preparation-induced browning supplies the missing absorption, and the ion-by-ion comparison provides compelling circumstantial evidence for a chemical shift — a comparison between the paired MO-OOA factors, online versus offline (Fig. 9). By every apportionment criterion the two are the same factor (matched spectra and time series; Sect. 2.4), yet their compositions differ subtly: across the matched ions,

https://doi.org/10.5194/egusphere-2026-5207
Preprint. Discussion started: 11 September 2026

the nitrogen families are enriched in the offline factor — $C_xH_yN^+$ by 1.6 and $C_xH_yNO_z^+$ by 1.5 — against the solubility-selection gradient. Reduced-N fragments derive from amines and N-heterocycles that are among the least oxidized constituents of the factor, so a water cut that strips $C_xH_y^+$ should deplete, not enrich, them. While the depletion of water-insoluble hydrocarbons mathematically increases the relative mass fractions of all surviving components, the disproportionate enrichment of reduced-N fragments (~1.6×) relative to oxygenated fragments (1.0–1.2×) points directly to chemical transformation rather than simple physical selection. Thus, this nitrogen enrichment serves as a strong empirical indicator of chromophore formation in the sample. Evaporating droplets strongly accelerate dehydration–condensation reactions (Nguyen et al., 2012), and aqueous carbonyls react with ammonium and amines to form imines and reduced-N heterocycles such as imidazoles (Bones et al., 2010; Updyke et al., 2012). Because such heterocycles are efficient chromophores, converting a trace of the factor's mass produces a large optical change: the same MO-OOA that is optically inert online (MAC 0.07 $m^2\ g^{-1}$) becomes an efficient absorber offline (0.88 $m^2\ g^{-1}$). The trace-mass argument equally shows that the apportionment is unaffected — the bulk spectra and factor time series are preserved, and only the MAC moves. Together, the two mechanisms suffice to reconcile the opposite absorption–O/C trends of the two platforms (Sect. 3.3.3).

3.3.3 Complementary measurement windows reconcile the opposite absorption–O/C trends

The two platforms are complementary rather than contradictory: the online measurement records the real-time optical state of the whole airborne particle, whereas the offline measurement records what a 24 h water extract retains after solubility selection and preparation chemistry (Sect. 3.3.2). This one distinction resolves the opposite absorption–O/C trends (Fig. 8a,b; the same divergence appears when the two absorptions are plotted against the MO-OOA mass fraction, Fig. 8c,d). Online, $b_{abs,BrC}$(370 nm) decreases as O/C rises — real photobleaching of the aging particle. Offline, $b_{abs,WS\text{-}BrC}$(365 nm) increases with O/C not because oxidation creates absorption, but because the two O/C axes are different quantities that share a label: online O/C tracks the aging of the airborne particle, whereas offline O/C indexes how much carbonyl-rich photochemical SOA — at once the reservoir of soluble N-chromophores and the feedstock for carbonyl–amine browning during extraction — the filter collected. The positive offline slope is therefore a property of the measurement window, not an optical property of the airborne aerosol.

The principal limitation of this framework is that the two offline branches cannot be fully separated with the present data: real, water-soluble atmospheric N-chromophores (nitroaromatics, imidazoles), which online averaging dilutes and daytime photochemistry bleaches, and reduced-N chromophores formed during preparation both contribute to the offline signal. Neither is spurious, and neither corresponds to atmospheric whole-particle browning; quantifying their relative shares requires the extraction and derivatization controls outlined in the Supplement (Sect. S4). Importantly, this ambiguity does not affect

https://doi.org/10.5194/egusphere-2026-5207
Preprint. Discussion started: 11 September 2026

the central conclusion. Both branches are properties of the measurement window rather than of atmospheric whole-particle browning, so under either attribution the offline platform reweights the source ranking toward the water-soluble, more-oxidized pool, and the online–offline reversal and its downwind-forcing consequence stand. Resolving the branch split — for which the extraction and derivatization controls of Sect. S4 are designed — would refine the mechanism but would not overturn the finding that the inferred source of BrC absorption is set by the measurement window rather than by the aerosol alone.

3.3.4 Scope of the reversal and relation to earlier coupling studies

The platforms differ in what particles they sample: the online AMS and aethalometer characterize submicron, non-refractory PM_1, whereas the offline filters collect $PM_{2.5}$. Coarse-mode (1–2.5 μm) chromophores are captured offline but not online, and the AMS does not detect refractory and "dark" BrC or tar balls, which can carry substantial short-wavelength absorption in biomass-burning aerosol (Corbin et al., 2019; Chakrabarty et al., 2023). If refractory BrC is present, the online BBOA MAC is a lower bound. In the Seoul residential-heating regime, tar-ball abundance is expected to be low, consistent with European wintertime wood-burning aerosol, where insoluble tar balls are negligible (Moschos et al., 2018; Rovira et al., 2026), although this remains to be verified. This size/volatility mismatch is a distinct, second-order contributor to the online–offline difference and does not by itself invert the ranking; the solubility weighting of Sect. 3.3.2 does.

Earlier coupling studies (Moschos et al., 2018; Navarro-Barboza et al., 2025; Rovira et al., 2026) reported broad consistency between measured and source-reconstructed BrC absorption, which might appear to contradict the reversal reported here. The difference is methodological: in each of those studies the absorption and the OA factors shared a single measurement window — Moschos et al. (2018) regressed the absorption of water-soluble filter extracts onto factors resolved from those same extracts, while Navarro-Barboza et al. (2025) and Rovira et al. (2026) regressed online aethalometer absorption onto factors from co-located online speciation measurements — so the chromophores and the mass experienced the same solubility cut and preparation history, and a window mismatch could not register. We instead deliberately compare across windows, online whole-particle absorption against offline water-soluble absorption, which is precisely the comparison a modeler makes when combining data of different types. Our result therefore does not overturn the earlier agreement; it isolates the previously-implicit assumption that the two measurement windows are interchangeable, and shows they are not for a secondary-influenced, high-nitrogen urban winter aerosol. Consistently, our own offline record reproduces the earlier 2016 Seoul offline result and the water-soluble literature (Fig. S9): the bulk picture is robust across methods, and only the source-level attribution is method-dependent.

https://doi.org/10.5194/egusphere-2026-5207
Preprint. Discussion started: 11 September 2026

East Asian winter is expected to maximize the divergence. Its high loading of aromatic and reduced-nitrogen precursors under high-NO_x, high-humidity, low-boundary-layer conditions maximizes both the nocturnal aqueous browning that offline filters preserve and the daytime photobleaching that online instruments capture. This is consistent with rapid ambient bleaching of water-soluble BrC observed in the East Asian outflow (Fang et al., 2023). We therefore predict the reversal to be largest in secondary-influenced, high-nitrogen urban winter regimes such as East Asia, and smaller in primary-biomass-burning-dominated regimes (much of Europe and North America) where the absorbing pool is more water-soluble and the diurnal competition weaker, a testable prediction for future co-located online–offline campaigns.

3.4 Implications for source-resolved BrC parameterizations and global context

Source-resolved MAC values derived from field data are increasingly folded into radiative-transfer and chemical-transport models (Fang et al., 2023; Navarro-Barboza et al., 2025; Rovira et al., 2026), yet Table 1 shows that the same aerosol yields opposite source rankings depending on whether the constraining data are online or offline. The consequence is not a shift in magnitude but in attribution: a parameterization built on offline water-soluble MAC assigns wintertime urban BrC absorption to highly-oxidized secondary OA and would predict absorption to grow as OA ages (browning with O/C); the online, in-situ evidence assigns the absorption to biomass burning and less-oxidized secondary OA and shows the oxidized pool bleaching, not browning, in the atmosphere. Because these imply opposite signs for the evolution of BrC absorption downwind of the source, the choice of measurement window can flip the sign of the modeled aging trend, not just its size, with corresponding consequences for where and at what altitude BrC forcing is placed.

3.4.1 A first-order radiative sensitivity

To bound the consequence of the source reversal, we propagate the two source-resolved parameterizations through a deliberately simple, transparent column calculation; we emphasize that these numbers are order-of-magnitude conceptual sensitivity estimates designed to illustrate the relative divergence in modeled aging trajectories, not a comprehensive radiative-transfer evaluation. Taking the campaign-mean BrC absorption coefficient at 370 nm (14.9 Mm^{-1}), a boundary-layer depth of 1 km, and the measured BrC absorption Ångström exponent (~5) to extrapolate the absorption spectrum, the solar-weighted (300–700 nm) column BrC absorption aerosol optical depth (AAOD) is ~5.7×10^{-3}. Applying a clear-sky simple forcing efficiency (Chylek and Wong, 1995; atmospheric transmittance 0.79, surface albedo 0.15) gives an instantaneous regional BrC absorption forcing of ~+0.34 W m^{-2} at the source.

The two measurement windows do not disagree on this initial value, they agree on the bulk burden (Sect. 3.3), but they imply opposite downwind evolution. Because increasing O/C is the standard proxy for

https://doi.org/10.5194/egusphere-2026-5207
Preprint. Discussion started: 11 September 2026

atmospheric aging, the two platforms encode opposite aging trends: online absorption falls as O/C rises (bleaching), offline absorption rises with O/C (apparent browning). Using a representative ambient BrC bleaching rate of k ~0.23 d^{-1} (Dasari et al., 2019; Fang et al., 2023), the online, in-situ evidence (photobleaching; $b_{abs,BrC}$(370 nm) falling with O/C) predicts the forcing to decay to ~+0.17 W m^{-2} after three days of transport, whereas an offline-constrained parameterization (browning; absorption growing with O/C) predicts it to rise to ~+0.68 W m^{-2} over the same interval, a factor of ~4 spread in the three-day-aged BrC absorption forcing and, critically, an opposite sign of the aging trend ($dF/dt < 0$ versus > 0; Fig. 10). Because regional and global BrC forcing is dominated by aged, transported aerosol rather than by fresh near-source emission, this sign ambiguity, set entirely by which measurement window constrains the model, propagates directly into where, at what altitude, and with what magnitude BrC exerts its forcing. Even at the order-of-magnitude level, this shows the measurement window is not a second-order calibration detail but a critical modeling assumption that can flip the sign of the modeled downwind BrC forcing trend.

Getting the source right matters because the emission controls, lifetime and injection altitude of the responsible source set BrC forcing: attributing winter urban absorption to long-lived, regionally-distributed MO-OOA implies a different mitigation lever and forcing distribution than attributing it to near-source, controllable biomass burning.

4 Conclusions

We set out to test whether online and offline source apportionment identify the same sources of BrC absorption for a single wintertime urban aerosol. In Seoul (winter 2018), BrC contributed ~25 % of aerosol absorption at 370 nm. In the ambient, online window the attribution is coherent: biomass burning is the most efficient absorber (MAC 5.66 m^2 g^{-1}) and the principal source of the nitrogen associated with absorption; a nocturnal secondary factor (LO-OOA2, 2.94 m^2 g^{-1}) carries nitrogen-associated BrC that accumulates overnight and is removed after sunrise; a daytime factor (LO-OOA1, 4.22 m^2 g^{-1}) absorbs without nitrogen enrichment and photobleaches; and the most oxidized factor is optically negligible (0.07 m^2 g^{-1}). Winter urban BrC is thus carried by fresh, largely reduced-nitrogen-associated material and is lost, not gained, with photochemical aging.

The same regression applied to the offline window (24 h $PM_{2.5}$ filters, water-soluble extracts) inverts this ranking: biomass-burning OA collapses (0.64 m^2 g^{-1}) and the most oxidized factor becomes the dominant water-soluble absorber (0.88 m^2 g^{-1}). Two mechanisms account for the inversion: solubility selection removes the water-insoluble strong absorbers, and we hypothesize that preparation-induced browning enriches the offline factor in reduced-nitrogen fragments (~1.6×) against the solubility-selection gradient, while the bulk composition and factor time series are preserved (Sect. 2.4). The opposite absorption–O/C

https://doi.org/10.5194/egusphere-2026-5207
Preprint. Discussion started: 11 September 2026

slopes of the two platforms follow from the same distinction — real-time particle aging versus the soluble subset a filter collects. The reversal is therefore a measurement-window effect, not an atmospheric change.

At the bulk level the two windows agree with each other and with the prior record (whole-particle MAE ~3.5 $m^2\ g^{-1}$; Kim et al., 2016; Fig. S9); only the source-level attribution is method-dependent. For models this difference is first-order and cautions against the direct mixing of online and offline BrC datasets without accounting for the measurement window. An offline-constrained parameterization assigns winter urban BrC to aged oxidized OA and lets absorption grow with aging, whereas the online evidence assigns it to biomass burning and fresh secondary OA and bleaches it downwind — opposite signs for the aging trend and, in a simple column estimate, a factor-of-~4 spread in the three-day-aged BrC forcing (Sect. 3.4.1).

These conclusions rest on one winter campaign at one urban-background site, and the online BrC retrieval carries the usual AAE-subtraction uncertainty (±6–7 percentage points in the 370 nm BrC fraction — 25.7 % at AAEBC = 1.0, and 18.4–32.4 % across AAEBC 0.9–1.1 and 880/950 nm reference wavelengths; source ranking unchanged, Table S4). Looking forward, we recommend that source-resolved BrC absorption be reported together with its measurement window — method, solubility class and integration time; that online, time-resolved attribution be preferred where the ambient optical state enters radiative calculations; and that offline speciation be used for chromophore identification with solubility and preparation effects explicitly controlled (Sect. S4). Co-located online–offline campaigns across seasons and in other high-nitrogen winter environments would test whether the reversal scales with reduced-nitrogen chemistry, as the mechanism predicts, and would make the measurement window a reported, correctable property of source-resolved BrC datasets rather than a hidden assumption.

Data availability

The measurement data and the analysis code used to produce the figures in this study are available from the corresponding author on reasonable request.

Author contributions

HK: conceptualization, funding acquisition, supervision, writing (original draft, review and editing). YC: formal analysis, offline-AMS and offline optical analysis.

https://doi.org/10.5194/egusphere-2026-5207
Preprint. Discussion started: 11 September 2026

Competing interests

HK is a member of the editorial board of Atmospheric Chemistry and Physics.

Acknowledgements

This work was supported by the National Research Foundation of Korea (NRF) grant funded by the Korea government (MSIT) (RS-2025-00514570) and by the Seoul National University (SNU) Creative-Pioneering Program for Young Researchers : 'Development of SMaRT-based aerosol measurement and analysis systems for the evaluation of climate change and health risk assessment'.(900-20250086)

References

Andreae, M. O. and Gelencsér, A.: Black carbon or brown carbon? The nature of light-absorbing carbonaceous aerosols, Atmos. Chem. Phys., 6, 3131–3148, https://doi.org/10.5194/acp-6-3131-2006, 2006.

Baek, K.-M., Park, E. H., Kang, H., Ji, M.-J., Park, H.-M., Heo, J., and Kim, H.: Seasonal characteristics of atmospheric water-soluble organic nitrogen in $PM_{2.5}$ in Seoul, Korea: Source and atmospheric processes of free amino acids and aliphatic amines, Sci. Total Environ., 811, 152335, https://doi.org/10.1016/j.scitotenv.2021.152335, 2022.

Bones, D. L., Henricksen, D. K., Mang, S. A., et al.: Appearance of strong absorbers and fluorophores in limonene-O_3 secondary organic aerosol due to NH_4^+-mediated chemical aging over long time scales, J. Geophys. Res., 115, D05203, https://doi.org/10.1029/2009JD012864, 2010.

Bozzetti, C., Daellenbach, K. R., Hueglin, C., Fermo, P., Sciare, J., Kasper-Giebl, A., Mazar, Y., Abbaszade, G., El Kazzi, M., Gonzalez, R., Shuster-Meiseles, T., Flasch, M., Wolf, R., Křepelová, A., Canonaco, F., Schnelle-Kreis, J., Slowik, J. G., Zimmermann, R., Rudich, Y., Baltensperger, U., El Haddad, I., and Prévôt, A. S. H.: Argon offline-AMS source apportionment of organic aerosol over yearly cycles for an urban, rural, and marine site in northern Europe, Atmos. Chem. Phys., 17, 117–141, https://doi.org/10.5194/acp-17-117-2017, 2017.

Canagaratna, M. R., Jimenez, J. L., Kroll, J. H., et al.: Elemental ratio measurements of organic compounds using aerosol mass spectrometry, Atmos. Chem. Phys., 15, 253–272, https://doi.org/10.5194/acp-15-253-2015, 2015.

Canonaco, F., Crippa, M., Slowik, J. G., Baltensperger, U., and Prévôt, A. S. H.: SoFi, an IGOR-based interface for the efficient use of the generalized multilinear engine (ME-2) for the source apportionment:

https://doi.org/10.5194/egusphere-2026-5207
Preprint. Discussion started: 11 September 2026

ME-2 application to aerosol mass spectrometer data, Atmos. Meas. Tech., 6, 3649–3661, https://doi.org/10.5194/amt-6-3649-2013, 2013.

Chakrabarty, R. K., Shetty, N. J., Thind, A. S., et al.: Shortwave absorption by wildfire smoke dominated by dark brown carbon, Nat. Geosci., 16, 683–688, https://doi.org/10.1038/s41561-023-01237-9, 2023.

Cheng, Y., Liu, C., Wang, J., Wang, J., Zhang, Z., Chen, L., Ge, D., Zhu, C., Wang, J., and Ding, A.: An observation-constrained estimation of brown carbon aerosol direct radiative effects, Atmos. Chem. Phys., 24, 3065–3078, https://doi.org/10.5194/acp-24-3065-2024, 2024.

Chylek, P. and Wong, J.: Effect of absorbing aerosols on global radiation budget, Geophys. Res. Lett., 22, 929–931, https://doi.org/10.1029/95GL00800, 1995.

Corbin, J. C., Czech, H., Massabò, D., et al.: Infrared-absorbing carbonaceous tar can dominate light absorption by marine-engine exhaust, npj Clim. Atmos. Sci., 2, 12, https://doi.org/10.1038/s41612-019-0069-5, 2019.

Crippa, M., Canonaco, F., Lanz, V. A., Äijälä, M., Allan, J. D., Carbone, S., Capes, G., Ceburnis, D., Dall'Osto, M., Day, D. A., et al.: Organic aerosol components derived from 25 AMS data sets across Europe using a consistent ME-2 based source apportionment approach, Atmos. Chem. Phys., 14, 6159–6176, https://doi.org/10.5194/acp-14-6159-2014, 2014.

Crippa, M., DeCarlo, P. F., Slowik, J. G., Mohr, C., Heringa, M. F., Chirico, R., Poulain, L., Freutel, F., Sciare, J., Cozic, J., Di Marco, C. F., et al.: Wintertime aerosol chemical composition and source apportionment of the organic fraction in the metropolitan area of Paris, Atmos. Chem. Phys., 13, 961–981, https://doi.org/10.5194/acp-13-961-2013, 2013.

Daellenbach, K. R., Bozzetti, C., Křepelová, A., Canonaco, F., Wolf, R., Zotter, P., Fermo, P., Crippa, M., Slowik, J. G., Sosedova, Y., Zhang, Y., Huang, R.-J., Poulain, L., Szidat, S., Baltensperger, U., El Haddad, I., and Prévôt, A. S. H.: Characterization and source apportionment of organic aerosol using offline aerosol mass spectrometry, Atmos. Meas. Tech., 9, 23–39, https://doi.org/10.5194/amt-9-23-2016, 2016.

Dasari, S., Andersson, A., Bikkina, S., et al.: Photochemical degradation affects the light absorption of water-soluble brown carbon in the South Asian outflow, Sci. Adv., 5, eaau8066, https://doi.org/10.1126/sciadv.aau8066, 2019.

DeCarlo, P. F., Kimmel, J. R., Trimborn, A., et al.: Field-deployable, high-resolution, time-of-flight aerosol mass spectrometer, Anal. Chem., 78, 8281–8289, https://doi.org/10.1021/ac061249n, 2006.

https://doi.org/10.5194/egusphere-2026-5207
Preprint. Discussion started: 11 September 2026

620 DeLessio, M. A., Tsigaridis, K., Bauer, S. E., Chowdhary, J., and Schuster, G. L.: Modeling atmospheric
621 brown carbon in the GISS ModelE Earth system model, Atmos. Chem. Phys., 24, 6275–6304,
622 https://doi.org/10.5194/acp-24-6275-2024, 2024.

623 Drinovec, L., Močnik, G., Zotter, P., et al.: The "dual-spot" Aethalometer, Atmos. Meas. Tech., 8, 1965–
624 1979, https://doi.org/10.5194/amt-8-1965-2015, 2015.

625 Fang, W., Andersson, A., Lee, M., Zheng, M., Du, K., Kim, S.-W., Holmstrand, H., and Gustafsson, Ö.:
626 Combined influences of sources and atmospheric bleaching on light absorption of water-soluble brown
627 carbon aerosols, npj Clim. Atmos. Sci., 6, 104, https://doi.org/10.1038/s41612-023-00438-8, 2023.

628 Hansen, A. D. A., Rosen, H., and Novakov, T.: The aethalometer, an instrument for the real-time
629 measurement of optical absorption by aerosol particles, Sci. Total Environ., 36, 191–196,
630 https://doi.org/10.1016/0048-9697(84)90265-1, 1984.

631 Haynes, J. P. J., Miller, K. E., and Majestic, B. J.: Investigation into photoinduced auto-oxidation of
632 polycyclic aromatic hydrocarbons resulting in brown carbon production, Environ. Sci. Technol., 53, 682–
633 691, https://doi.org/10.1021/acs.est.8b05704, 2019.

634 Hems, R. F. and Abbatt, J. P. D.: Aqueous phase photo-oxidation of brown carbon nitrophenols, ACS Earth
635 Space Chem., 2, 225–234, https://doi.org/10.1021/acsearthspacechem.7b00123, 2018.

636 Huang, X.-F., He, L.-Y., Xue, L., Sun, T.-L., Zeng, L.-W., Gong, Z.-H., Hu, M., and Zhu, T.: Highly time-
637 resolved chemical characterization of atmospheric fine particles during 2010 Shanghai World Expo, Atmos.
638 Chem. Phys., 12, 4897–4907, https://doi.org/10.5194/acp-12-4897-2012, 2012.

639 Iinuma, Y., Böge, O., Gräfe, R., and Herrmann, H.: Methyl-nitrocatechols: atmospheric tracer compounds
640 for biomass burning secondary organic aerosols, Environ. Sci. Technol., 44, 8453–8459,
641 https://doi.org/10.1021/es102938a, 2010.

642 IPCC: Climate Change 2013: The Physical Science Basis, Cambridge University Press, 2013.

643 Kasthuriarachchi, N. Y., Rivellini, L.-H., Chen, X., Li, Y.-J., and Lee, A. K. Y.: Light absorbing properties
644 of primary and secondary brown carbon in a tropical urban environment, Environ. Sci. Technol., 54, 10808–
645 10819, https://doi.org/10.1021/acs.est.0c02414, 2020.

646 Kim, H., et al.: Seasonal characteristics of the light absorption of water-soluble organic carbon in Seoul,
647 Atmos. Environ., 129, 234–242, https://doi.org/10.1016/j.atmosenv.2016.01.042, 2016.

https://doi.org/10.5194/egusphere-2026-5207
Preprint. Discussion started: 11 September 2026

Kuang, Y., Luo, B., Huang, S., Liu, J., Hu, W., Peng, Y., Chen, D., Yue, D., Xu, W., Yuan, B., and Shao, M.: Formation of highly absorptive secondary brown carbon through nighttime multiphase chemistry of biomass burning emissions, Atmos. Chem. Phys., 25, 3737–3752, https://doi.org/10.5194/acp-25-3737-2025, 2025.

Laskin, A., Laskin, J., and Nizkorodov, S. A.: Chemistry of atmospheric brown carbon, Chem. Rev., 115, 4335–4382, https://doi.org/10.1021/cr5006167, 2015.

Laskin, A., West, C. P., and Hettiyadura, A. P. S.: Molecular insights into the composition, sources, and aging of atmospheric brown carbon, Chem. Soc. Rev., 54, 1583–1612, https://doi.org/10.1039/D3CS00609C, 2025.

Li, Q., Jiang, X., Tian, P., et al.: Concurrent photochemical whitening and darkening of ambient brown carbon, Atmos. Chem. Phys., 23, 9439–9453, https://doi.org/10.5194/acp-23-9439-2023, 2023.

Li, Y. J., Lee, B. P., Su, L., Fung, J. C. H., and Chan, C. K.: Seasonal characteristics of fine particulate matter (PM) based on high-resolution time-of-flight aerosol mass spectrometric (HR-ToF-AMS) measurements at the HKUST Supersite in Hong Kong, Atmos. Chem. Phys., 15, 37–53, https://doi.org/10.5194/acp-15-37-2015, 2015.

Li, Y., Fu, T.-M., Yu, J. Z., Zhang, A., Yu, X., Ye, J., Zhu, L., Shen, H., Wang, C., Yang, X., Tao, S., Chen, Q., Li, Y., Li, L., Che, H., and Heald, C. L.: Nitrogen dominates global atmospheric organic aerosol absorption, Science, 387, 989–995, https://doi.org/10.1126/science.adr4473, 2025.

Lin, P., Bluvshtein, N., Rudich, Y., Nizkorodov, S. A., Laskin, J., and Laskin, A.: Molecular chemistry of atmospheric brown carbon inferred from a nationwide biomass burning event, Environ. Sci. Technol., 51, 11561–11570, https://doi.org/10.1021/acs.est.7b02276, 2017.

Mohr, C., DeCarlo, P. F., Heringa, M. F., Chirico, R., Slowik, J. G., Richter, R., Reche, C., Alastuey, A., Querol, X., Seco, R., Peñuelas, J., et al.: Identification and quantification of organic aerosol from cooking and other sources in Barcelona using aerosol mass spectrometer data, Atmos. Chem. Phys., 12, 1649–1665, https://doi.org/10.5194/acp-12-1649-2012, 2012.

Mohr, C., Lopez-Hilfiker, F. D., Zotter, P., Prévôt, A. S. H., Xu, L., Ng, N. L., et al.: Contribution of nitrated phenols to wood burning brown carbon light absorption in Detling, United Kingdom during winter time, Environ. Sci. Technol., 47, 6316–6324, https://doi.org/10.1021/es400683v, 2013.

Moschos, V., Gysel-Beer, M., Modini, R. L., Corbin, J. C., Massabò, D., Costa, C., Danelli, S. G., Vlachou, A., Daellenbach, K. R., Szidat, S., Prati, P., Prévôt, A. S. H., Baltensperger, U., and El Haddad, I.: Source-

https://doi.org/10.5194/egusphere-2026-5207
Preprint. Discussion started: 11 September 2026

specific light absorption by carbonaceous components in the complex aerosol matrix from yearly filter-based measurements, Atmos. Chem. Phys., 21, 12809–12833, https://doi.org/10.5194/acp-21-12809-2021, 2021.

Moschos, V., Kumar, N. K., Daellenbach, K. R., Baltensperger, U., Prévôt, A. S. H., and El Haddad, I.: Source apportionment of brown carbon absorption by coupling ultraviolet–visible spectroscopy with aerosol mass spectrometry, Environ. Sci. Technol. Lett., 5, 302–308, https://doi.org/10.1021/acs.estlett.8b00118, 2018.

Navarro-Barboza, H., et al.: Characterization of brown carbon absorption in different European environments through source contribution analysis, Atmos. Chem. Phys., 25, 2667–2694, https://doi.org/10.5194/acp-25-2667-2025, 2025.

Nguyen, T. B., Lee, P. B., Updyke, K. M., et al.: Formation of nitrogen- and sulfur-containing light-absorbing compounds accelerated by evaporation of water from secondary organic aerosols, J. Geophys. Res., 117, D01207, https://doi.org/10.1029/2011JD016944, 2012.

Paatero, P. and Tapper, U.: Positive matrix factorization: a non-negative factor model with optimal utilization of error estimates of data values, Environmetrics, 5, 111–126, https://doi.org/10.1002/env.3170050203, 1994.

Pieber, S. M., El Haddad, I., Slowik, J. G., Canagaratna, M. R., Jayne, J. T., Platt, S. M., Bozzetti, C., Daellenbach, K. R., Fröhlich, R., Vlachou, A., et al.: Inorganic salt interference on CO_2^+ in Aerodyne AMS and ACSM organic aerosol composition studies, Environ. Sci. Technol., 50, 10494–10503, https://doi.org/10.1021/acs.est.6b01035, 2016.

Qin, Y. M., et al.: Chemical characteristics of brown carbon in atmospheric particles at a suburban site near Guangzhou, China, Atmos. Chem. Phys., 18, 16409–16427, https://doi.org/10.5194/acp-18-16409-2018, 2018.

Qiu, Y., et al.: Understanding divergent brown carbon photobleaching rates, Atmos. Chem. Phys., 26, 2785–…, 2026.

Rana, M. S. and Guzman, M. I.: Oxidation of catechols at the air–water interface by nitrate radicals, Environ. Sci. Technol., 56, 15437–15448, https://doi.org/10.1021/acs.est.2c05640, 2022.

Rana, M. S. and Guzman, M. I.: Oxidation of catechols at the air–water interface by nitrate radicals, Environ. Sci. Technol., 56, 15437–15448, https://doi.org/10.1021/acs.est.2c05640, 2022.

https://doi.org/10.5194/egusphere-2026-5207
Preprint. Discussion started: 11 September 2026

Ren, Y., Wu, Z., Ji, Y., Bi, F., Li, J., Zhang, H., Zhang, H., Li, H., and Wang, G.: Non-negligible secondary contribution to brown carbon in autumn and winter: inspiration from particulate nitrated and oxygenated aromatic compounds in urban Beijing, Atmos. Chem. Phys., 24, 6525–6538, https://doi.org/10.5194/acp-24-6525-2024, 2024.

Rovira, J., Yus-Díez, J., Chen, G. I., et al.: Constraining the intensive absorption properties of ambient organic aerosol particles based on pan-European observations, npj Clim. Atmos. Sci., 9, 131, https://doi.org/10.1038/s41612-026-01405-9, 2026.

Saleh, R., Robinson, E. S., Tkacik, D. S., et al.: Brownness of organics in aerosols from biomass burning linked to their black carbon content, Nat. Geosci., 7, 647–650, https://doi.org/10.1038/ngeo2220, 2014.

Tang, J., Wang, J., Zhong, G., Jiang, H., Mo, Y., Zhang, B., Geng, X., Chen, Y., Tang, J., Tian, C., Bualert, S., Li, J., and Zhang, G.: Measurement report: Long-emission-wavelength chromophores dominate the light absorption of brown carbon in aerosols over Bangkok, Atmos. Chem. Phys., 21, 11337–11352, https://doi.org/10.5194/acp-21-11337-2021, 2021.

Ulbrich, I. M., Canagaratna, M. R., Zhang, Q., Worsnop, D. R., and Jimenez, J. L.: Interpretation of organic components from Positive Matrix Factorization of aerosol mass spectrometric data, Atmos. Chem. Phys., 9, 2891–2918, https://doi.org/10.5194/acp-9-2891-2009, 2009.

Updyke, K. M., Nguyen, T. B., and Nizkorodov, S. A.: Formation of brown carbon via reactions of ammonia with secondary organic aerosols from biogenic and anthropogenic precursors, Atmos. Environ., 63, 22–31, https://doi.org/10.1016/j.atmosenv.2012.09.012, 2012.

Wang, D., Shen, Z., Zhang, Q., Lei, Y., Zhang, T., Huang, S., Sun, J., Xu, H., and Cao, J.: Winter brown carbon over six of China's megacities: light absorption, molecular characterization, and improved source apportionment revealed by multilayer perceptron neural network, Atmos. Chem. Phys., 22, 14893–14913, https://doi.org/10.5194/acp-22-14893-2022, 2022.

Wong, J. P. S., Tsagkaraki, M., Tsiodra, I., et al.: Atmospheric evolution of molecular-weight-separated brown carbon from biomass burning, Atmos. Chem. Phys., 19, 7319–7334, https://doi.org/10.5194/acp-19-7319-2019, 2019.

Xu, J., Shi, J., Zhang, Q., Ge, X., Canonaco, F., Prévôt, A. S. H., Vonwiller, M., Szidat, S., Ge, J., Ma, J., An, Y., Kang, S., and Qin, D.: Wintertime organic and inorganic aerosols in Lanzhou, China: sources, processes, and comparison with the results during summer, Atmos. Chem. Phys., 16, 14937–14952, https://doi.org/10.5194/acp-16-14937-2016, 2016.

https://doi.org/10.5194/egusphere-2026-5207
Preprint. Discussion started: 11 September 2026

737 Xu, L., Guo, H., Boyd, C. M., Klein, M., Bougiatioti, A., Cerully, K. M., Hite, J. R., Isaacman-VanWertz,
738 G., Kreisberg, N. M., Knote, C., et al.: Effects of anthropogenic emissions on aerosol formation from
739 isoprene and monoterpenes in the southeastern United States, Proc. Natl. Acad. Sci. USA, 112, 37–42,
740 https://doi.org/10.1073/pnas.1417609112, 2015.

741 Yan, C. Q., Zheng, M., Bosch, C., Andersson, A., Desyaterik, Y., Sullivan, A. P., Collett, J. L., Zhao, B.,
742 Wang, S. X., He, K. B., and Gustafsson, Ö.: Important fossil source contribution to brown carbon in Beijing
743 during winter, Sci. Rep., 7, 43182, https://doi.org/10.1038/srep43182, 2017.

744 Yang, Y., et al.: Laboratory studies on the optical, physical, and chemical properties of fresh and aged
745 biomass burning aerosols, Atmos. Chem. Phys., 25, 11051–11069, https://doi.org/10.5194/acp-25-11051-
746 2025, 2025.

747 Yuan, W., Huang, R.-J., Yang, L., Guo, J., Chen, Z., Duan, J., Wang, T., Ni, H., Han, Y., Li, Y., Chen, Q.,
748 Chen, Y., Hoffmann, T., and O'Dowd, C.: Characterization of the light-absorbing properties, chromophore
749 composition and sources of brown carbon aerosol in Xi'an, northwestern China, Atmos. Chem. Phys., 20,
750 5129–5144, https://doi.org/10.5194/acp-20-5129-2020, 2020.

751 Zhang, Q., Jimenez, J. L., Canagaratna, M. R., Ulbrich, I. M., Ng, N. L., Worsnop, D. R., and Sun, Y.:
752 Understanding atmospheric organic aerosols via factor analysis of aerosol mass spectrometry: a review,
753 Anal. Bioanal. Chem., 401, 3045–3067, https://doi.org/10.1007/s00216-011-5355-y, 2011a.

754 Zhang, X., Lin, Y.-H., Surratt, J. D., Zotter, P., Prévôt, A. S. H., and Weber, R. J.: Light-absorbing soluble
755 organic aerosol in Los Angeles and Atlanta: A contrast in secondary organic aerosol, Geophys. Res. Lett.,
756 38, L21810, https://doi.org/10.1029/2011GL049385, 2011b.

757 Zhang, X., Lin, Y.-H., Surratt, J. D., and Weber, R. J.: Sources, composition and absorption Ångström
758 exponent of light-absorbing organic components in aerosol extracts (SE US), Atmos. Environ., 140, 15–
759 27, https://doi.org/10.1016/j.atmosenv.2016.05.055, 2016.

760 Zhang, X., Lin, Y.-H., Surratt, J. D., Zotter, P., Prévôt, A. S. H., and Weber, R. J.: Light-absorbing soluble
761 organic aerosol in Los Angeles and Atlanta: A contrast in secondary organic aerosol, Geophys. Res. Lett.,
762 38, L21810, https://doi.org/10.1029/2011GL049385, 2011.

763 Zhao, R., Lee, A. K. Y., Huang, L., et al.: Photochemical processing of aqueous atmospheric brown carbon,
764 Atmos. Chem. Phys., 15, 6087–6100, https://doi.org/10.5194/acp-15-6087-2015, 2015.

765

766

https://doi.org/10.5194/egusphere-2026-5207
Preprint. Discussion started: 11 September 2026

Figures

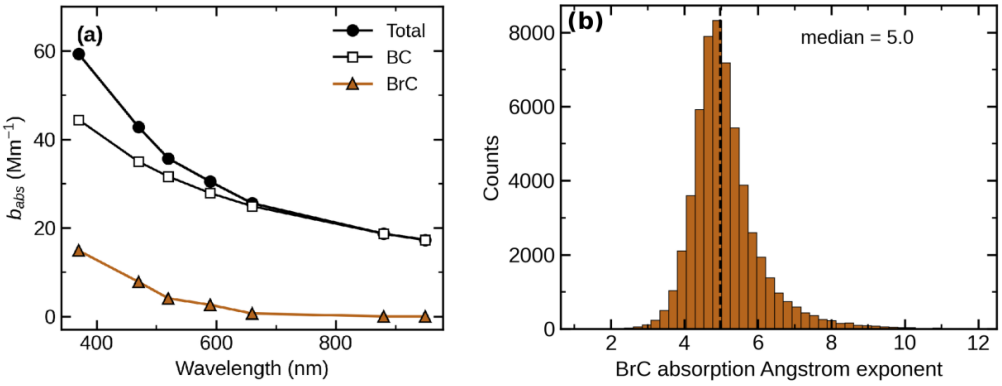

Figure 1. Presence of light-absorbing organic aerosol at the Seoul urban-background site. (a) Campaign-mean seven-wavelength aethalometer absorption coefficient b_{abs} (370–950 nm; AE33 dual-spot aethalometer, filter-loading corrected in real time following Hansen et al. (1984) and Drinovec et al. (2015)), decomposed into the black-carbon (BC, open squares) and brown-carbon (BrC, filled triangles) components, with BC obtained by extrapolating the 880 nm signal at an assumed BC absorption Ångström exponent of 1.0 and BrC taken as the residual. (b) Distribution of the brown-carbon absorption Ångström exponent (AAE, fitted over 370–660 nm) over the campaign; the median (~5.0; dashed line) is the fingerprint of aged, secondary-influenced urban BrC rather than fresh primary emission.

https://doi.org/10.5194/egusphere-2026-5207
Preprint. Discussion started: 11 September 2026

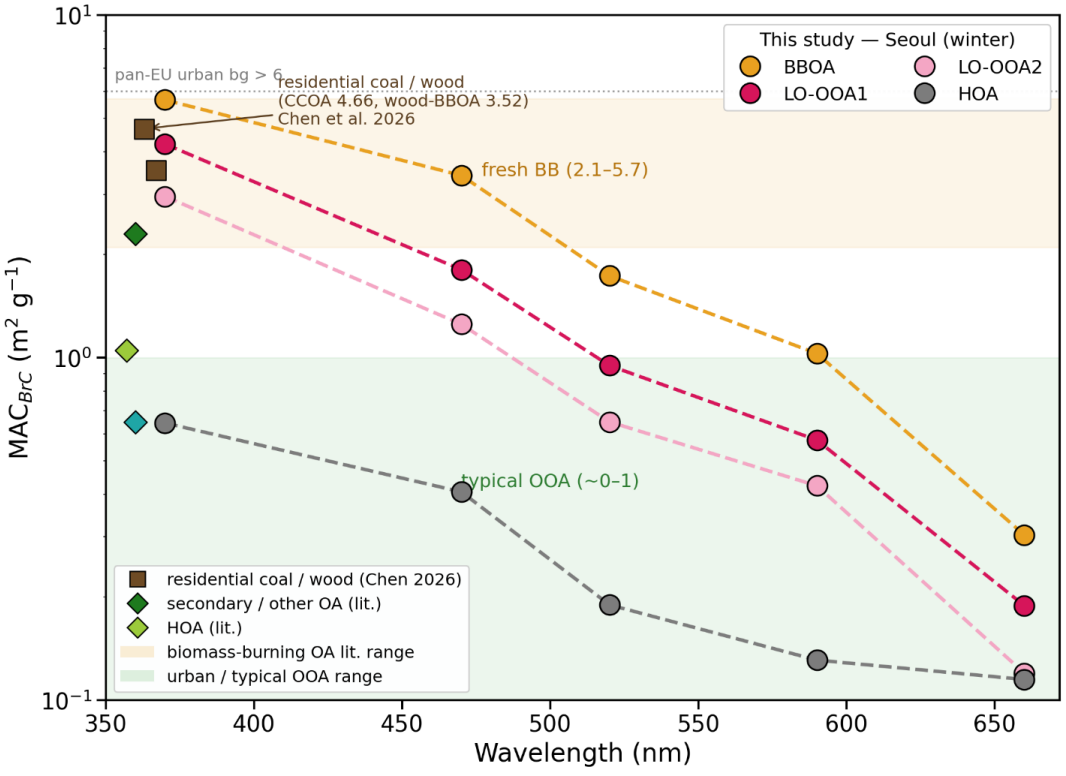

Figure 2. Source-resolved brown carbon mass absorption cross-section and its consistency with the literature. Wavelength dependence (370–660 nm) of MAC_{BrC} for the four absorbing online OA factors — BBOA (orange), LO-OOA1 (magenta), LO-OOA2 (pink) and HOA (grey) — retrieved by origin-forced multiple linear regression of the aethalometer BrC absorption onto the PMF factor mass time series (dashed lines with filled circles); MO-OOA and COA were optically negligible and are omitted. Shaded horizontal bands mark literature MAC ranges at 370 nm for fresh biomass-burning OA (2.1–5.7 m² g⁻¹; Yang et al., 2025; orange) and for typical bulk oxidized/urban OOA (~0–1 m² g⁻¹; green). Overlaid symbols are published single-factor MAC values at 370 nm: residential-coal (CCOA, 4.66) and wood-burning BBOA (3.52) from the pan-European dataset (Rovira et al., 2026; squares); strongly-absorbing secondary "Night-OA" (2.3; Kuang et al., 2025), LV-OOA (1.04; Qin et al., 2018), water-soluble OOA (0.7; Moschos et al., 2021) and low-absorbing OA (0.13) as diamonds, and HOA (0.24; triangle). The Seoul BBOA (5.7 m² g⁻¹) falls within the fresh-biomass-burning and pan-European residential-combustion range, the less-oxidized secondary factors (LO-OOA1 4.2, LO-OOA2 3.0) lie well above the typical-OOA band and match strongly-absorbing secondary BrC reported elsewhere, and HOA (0.7) is within the literature range — confirming the resolved factors are physically reasonable absorbers rather than regression artifacts. All literature values are taken at 370 nm.

https://doi.org/10.5194/egusphere-2026-5207
Preprint. Discussion started: 11 September 2026

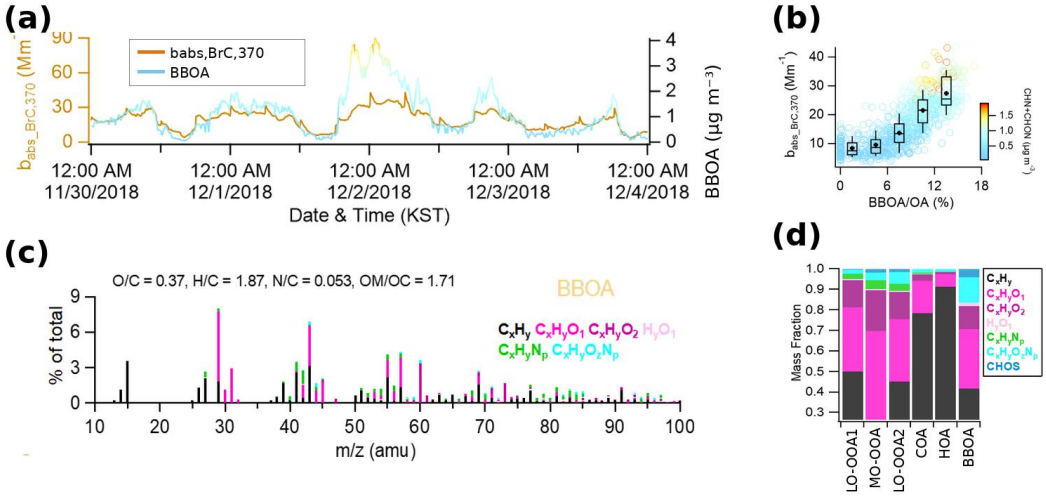

Figure 3. Biomass-burning impact on BrC absorption and its nitrogen signature. (a) Time series of whole-particle BrC absorption $b_{abs,BrC}$ at 370 nm (orange) and BBOA mass concentration (light blue); absorption maxima coincide with the biomass-burning episodes. (b) $b_{abs,BrC}$ at 370 nm versus the BBOA mass fraction of OA, coloured by the summed CHN + CHON concentration; overlaid boxes are binned medians and quartiles. (c) High-resolution BBOA factor mass spectrum, colored by ion family, with the factor elemental ratios (O/C = 0.37, H/C = 1.87, N/C = 0.053, OM/OC = 1.71). (d) Ion-family mass fractions of OA binned by BBOA/OA; the nitrogen-containing families ($C_xH_yN^+$, $C_xH_yNO_z^+$) increase with the biomass-burning fraction (highlighted bin).

https://doi.org/10.5194/egusphere-2026-5207
Preprint. Discussion started: 11 September 2026

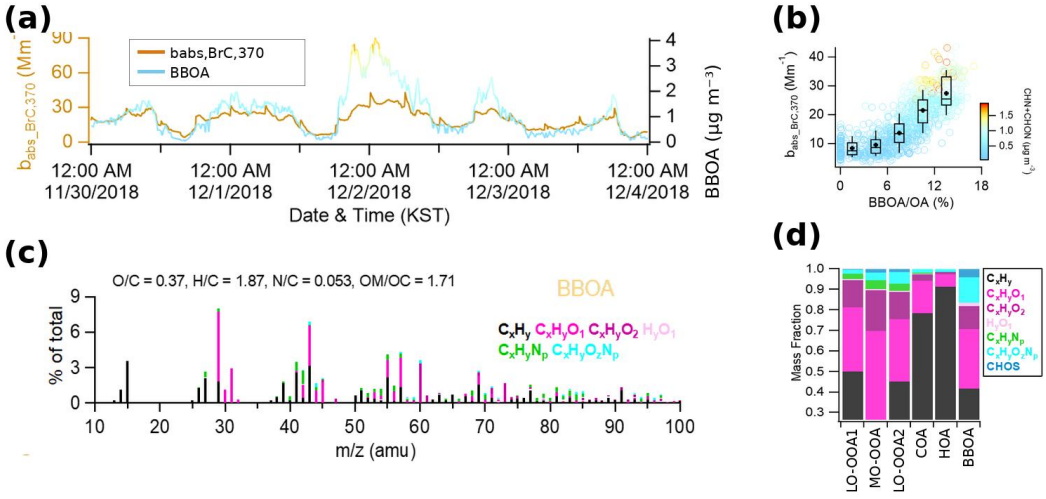

Figure 4. Nighttime secondary BrC absorption is nitrogen-associated. (a) Whole-particle BrC absorption $b_{abs,BrC}$ at 370 nm versus the nighttime secondary factor LO-OOA2 ($r^2 = 0.45$) and versus LO-OOA1 ($r^2 = 0.10$); marker colour scales with the $C_xH_yN^+$ loading. (b) Pearson correlation (r) of each online factor's time series with individual ions: LO-OOA2 and BBOA correlate strongly and positively with the nitrogen-containing organic fragments ($C_xH_yN^+$; r ~0.58–0.86 and 0.65–0.90, respectively), whereas LO-OOA1 is uncorrelated-to-negative, so its absorption is not nitrogen-driven. (c) Mean diurnal cycles (local time). Top: mean mass concentrations of the three secondary factors — LO-OOA1 and LO-OOA2 (left axis) and MO-OOA (right axis). Bottom: the primary and secondary contributions to BrC absorption at 370 nm (BrC_Pri, grey; BrC_Sec, orange), with the whole-particle $b_{abs,BrC}$(370 nm) (open circles, right axis) and the incident solar radiation (filled circles, far-right axis). BrC absorption and LO-OOA2 both rise through the night, when a shallow boundary layer and high relative humidity favour aqueous processing and the secondary share of BrC absorption is largest then, whereas MO-OOA peaks near midday with solar radiation, when photobleaching drives whole-particle BrC absorption to its minimum.

https://doi.org/10.5194/egusphere-2026-5207
Preprint. Discussion started: 11 September 2026

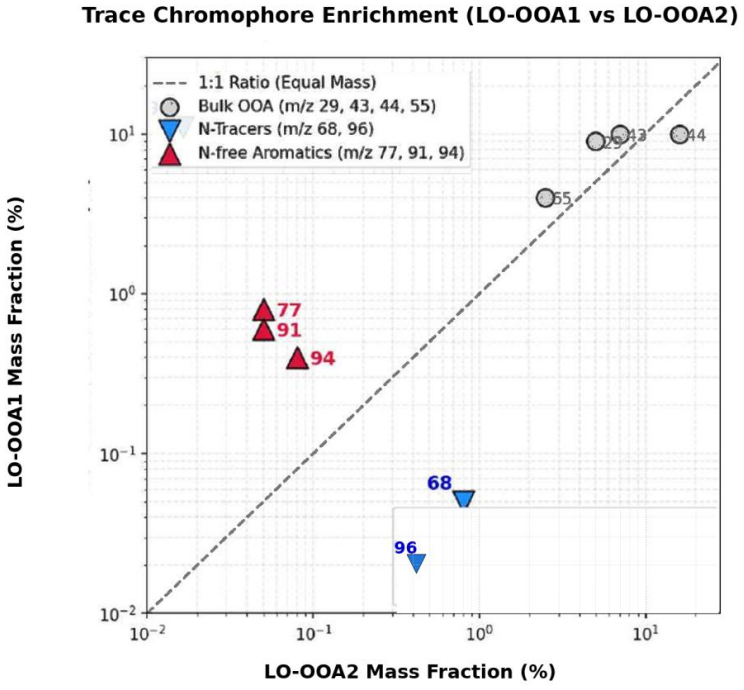

Figure 5. LO-OOA1 absorbs without nitrogen. Ion-by-ion mass-fraction comparison of LO-OOA1 versus LO-OOA2: the non-nitrogenous aromatic fragments *m/z* 77, 91 and 94 (red triangles) are enriched in LO-OOA1 (above the 1:1 line), whereas the nitrogen tracers *m/z* 68 and 96 (blue) are depleted — indicating LO-OOA1's absorption arises from non-nitrogenous aromatics.

https://doi.org/10.5194/egusphere-2026-5207
Preprint. Discussion started: 11 September 2026

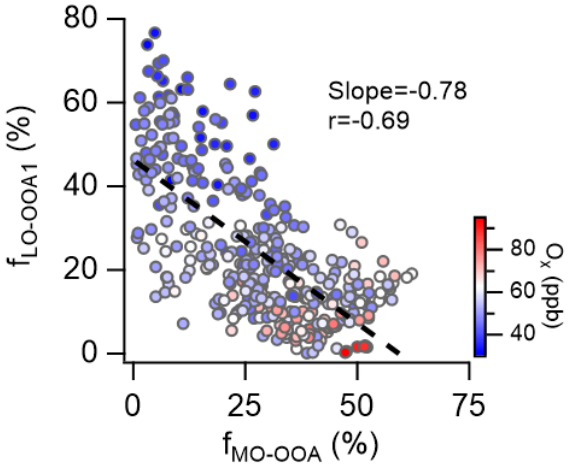

Figure 6. Daytime photobleaching of the online aerosol. Daytime anti-correlation between the LO-OOA1 and MO-OOA fractional contributions to OA, with each point coloured by odd oxygen ($O_x = O_3 + NO_2$), a photochemical-age proxy (slope = −0.78, r = −0.69): as O_x increases, the absorbing LO-OOA1 fraction falls while the more-oxidized, non-absorbing MO-OOA fraction rises, tracing the daytime conversion of LO-OOA1 to MO-OOA.

https://doi.org/10.5194/egusphere-2026-5207
Preprint. Discussion started: 11 September 2026

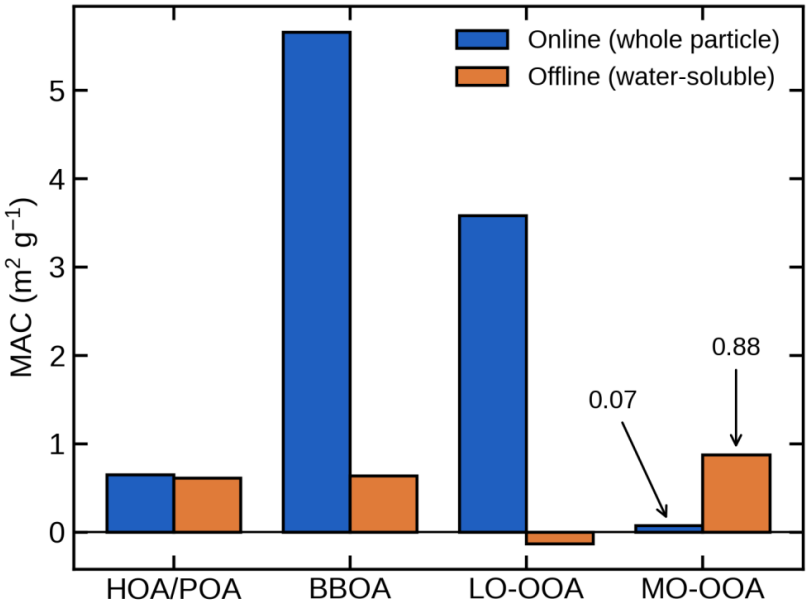

Figure 7. The online–offline source reversal. Source-resolved MAC from the online (whole-particle, 370 nm) and offline (water-soluble, 365 nm) platforms applied to the same aerosol (values in Table 1; bootstrap 95 % confidence intervals, VIFs and the NNLS refit in Table S3). The ranking inverts: MO-OOA is optically negligible online (0.07 $m^2\ g^{-1}$) but the dominant water-soluble absorber offline (0.88 $m^2\ g^{-1}$), while BBOA collapses from 5.66 to 0.64 $m^2\ g^{-1}$. The online and offline MO-OOA time series nonetheless track closely (Fig. S5), confirming they are the same factor.

https://doi.org/10.5194/egusphere-2026-5207
Preprint. Discussion started: 11 September 2026

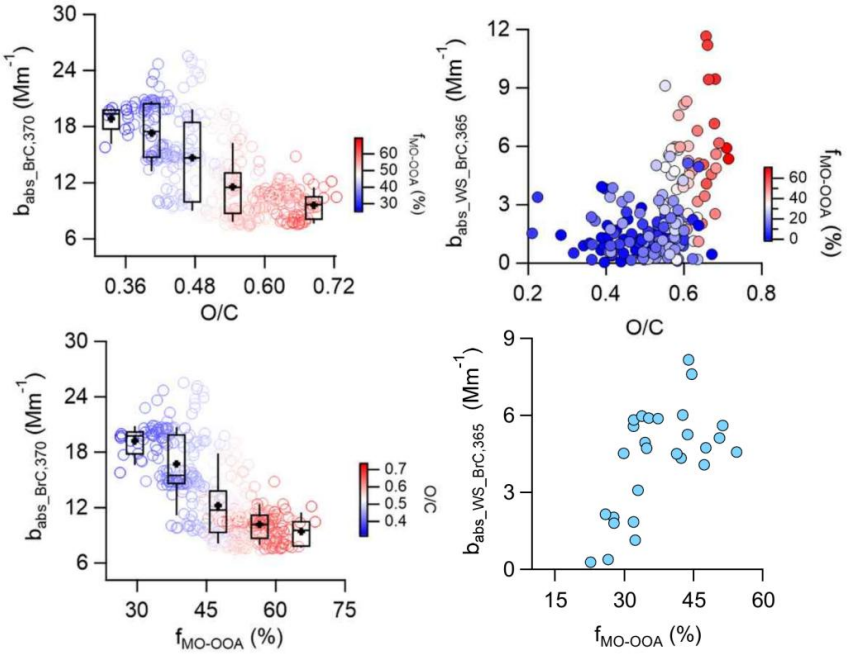

Figure 8. Opposite absorption–O/C trends in the online and offline platforms. (a) Online whole-particle BrC absorption $b_{abs,BrC}$ at 370 nm versus O/C, coloured by the MO-OOA mass fraction f_{MO-OOA}; $b_{abs,BrC}$(370 nm) decreases as O/C rises — real-time photobleaching of the aging particle (Pearson r ~−0.30). (b) Offline water-soluble BrC absorption $b_{abs,WS-BrC}$ at 365 nm versus O/C, coloured by f_{MO-OOA}; $b_{abs,WS-BrC}$(365 nm) increases with O/C (r ~+0.45). (c, d) The same online and offline absorption plotted against f_{MO-OOA}. Box overlays mark binned medians and quartiles. The two O/C axes are different quantities that share a label: online O/C tracks the real-time aging of one particle, whereas offline O/C indexes which water-soluble subset a 24 h filter collected (Sect. 3.3).

https://doi.org/10.5194/egusphere-2026-5207
Preprint. Discussion started: 11 September 2026

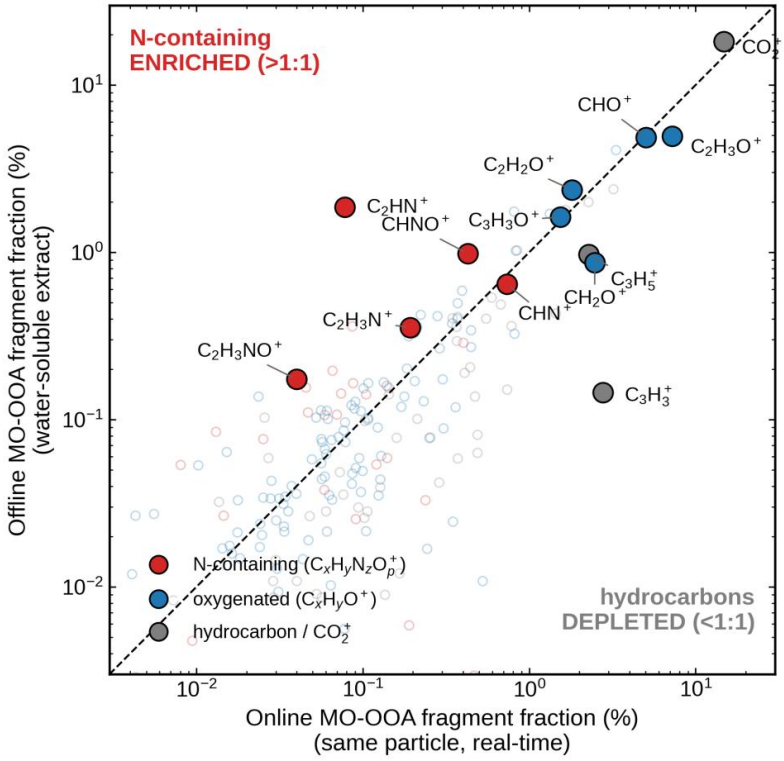

862

863 **Figure 9.** The offline MO-OOA is chemically shifted, not merely re-selected. Ion-by-ion comparison, on log–log axes
864 with equal ranges, of the fragment contributions to the online (real-time, whole-particle) and offline (24 h water-
865 soluble extract) MO-OOA high-resolution mass spectra (n = 241 matched ions; faint open circles show every matched
866 ion, filled symbols the labelled major fragments), with the 1:1 line dashed. Symbols are coloured by ion family:
867 nitrogen-containing ($C_xH_yNO_z^+$; red), oxygenated ($C_xH_yO^+$; blue) and hydrocarbon or CO_2^+ (grey). Nitrogen-
868 containing fragments lie systematically above the 1:1 line (enriched offline; family ratio ~1.5–1.6; e.g. C_2HN^+,
869 $CHNO^+$, $C_2H_3N^+$, $C_2H_3NO^+$), whereas hydrocarbon fragments fall below it (depleted, ratio 0.54; e.g. $C_3H_3^+$, $C_3H_5^+$,
870 CH_2O^+) and CO_2^+ sits near the line. Because the nitrogen enrichment runs opposite to the water-soluble selection
871 gradient that strips the chemically similar hydrocarbon fragments, it cannot be produced by solubility selection and is
872 the fingerprint of reduced-nitrogen chromophores formed during extraction, atomization and drying (Sect. 3.3; the
873 aqueous carbonyl–amine chemistry follows Nguyen et al., 2012; Bones et al., 2010; Updyke et al., 2012). That the
874 offline and online MO-OOA factor mass concentrations nonetheless track closely (Fig. S5) confirms the two are the
875 same factor and that only the trace-chromophore composition, not the bulk mass, is shifted.

https://doi.org/10.5194/egusphere-2026-5207
Preprint. Discussion started: 11 September 2026

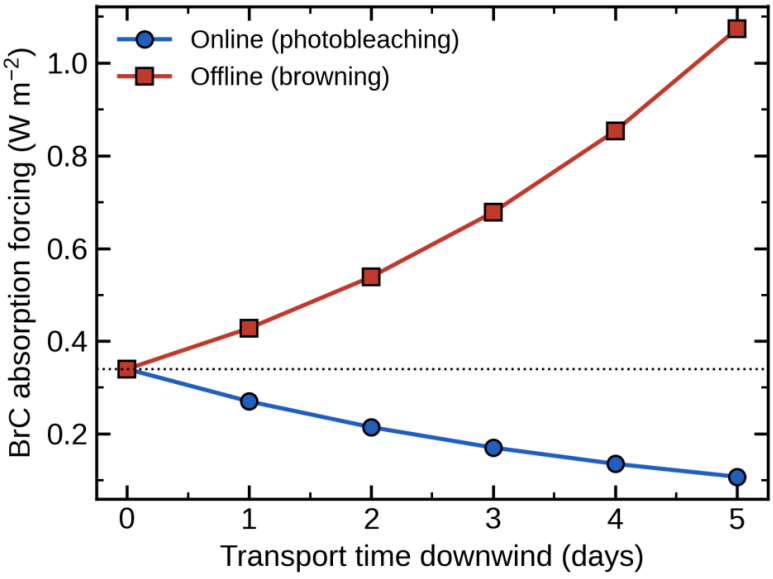

Figure 10. First-order radiative sensitivity to the measurement window. Instantaneous regional clear-sky BrC absorption forcing at the source (~+0.34 W m^{-2}; simple column estimate, Sect. 3.4.1) and its downwind evolution under the online-constrained (photobleaching) and offline-constrained (browning) source parameterizations, using an ambient water-soluble BrC bleaching rate k = 0.23 d^{-1} (Dasari et al., 2019; Fang et al., 2023). The two windows agree at the source but diverge by a factor of ~4 after three days and give opposite signs for the aging trend (dF/dt < 0 vs > 0). Assumptions: boundary-layer depth 1 km, BrC AAE ~5, atmospheric transmittance 0.79, surface albedo 0.15, clear sky; simple forcing efficiency after Chylek and Wong (1995). Data are from this study.

https://doi.org/10.5194/egusphere-2026-5207
Preprint. Discussion started: 11 September 2026

Tables

Table 1. Source-resolved BrC mass absorption coefficient (MAC, $m^2\ g^{-1}$) from origin-forced multiple linear regression of bulk absorption onto the PMF factor mass time series, for the online ($b_{abs,BrC}$ at 370 nm) and offline ($b_{abs,WS\text{-}BrC}$ at 365 nm) platforms. Bootstrap 95 % confidence intervals, variance-inflation factors and a non-negative least-squares refit are given in Table S3. The two platforms agree on the qualitative bulk attribution but invert the source ranking.

OA factor	Online MAC, 370 nm ($m^2\ g^{-1}$)	Offline WSOA MAC, 365 nm ($m^2\ g^{-1}$)
HOA / POA	0.65	0.61
BBOA	5.66	0.64
LO-OOA1	4.22	~0 (LO-OOA, combined)
LO-OOA2	2.94	—
MO-OOA	0.07	0.88

https://doi.org/10.5194/egusphere-2026-5207
Preprint. Discussion started: 11 September 2026

Table 2. Source-resolved contribution to brown-carbon light absorption ($b_{abs,BrC}$) across urban and regional sites, integrating a mixed-season single-site compilation with season-matched winter East Asia. For the compiled single-site studies, the contribution of each source to BrC absorption is obtained by weighting the OA-factor mass fractions reported in the cited study by this study's measured factor mass absorption coefficients at 370 nm — combustion (biomass-burning/coal) 5.66, less-oxidized secondary (LO-/SV-OOA) 3.5, more-oxidized secondary (MO-/LV-OOA) 0.07, and other primary (HOA/O-HOA/COA) 0.5 $m^2\ g^{-1}$ — and normalizing to 100 % (underlying mass fractions in Table S5; Paris OOA, reported combined, split 50:50, and isoprene-OA at Centreville treated as optically weak). Seoul is this study's measured MLR attribution. Wang et al. (2022) values are directly source-apportioned BrC absorption at 365 nm, with "combustion" = biomass-burning share and "other primary" = total primary − biomass burning; n.r. = not resolved. Independent ^{14}C radiocarbon apportionment assigns 67 ± 3 % of Beijing's light-absorbing organic carbon to fossil, coal-dominated combustion (Yan et al., 2017). Secondary absorption is carried almost entirely by the less-oxidized factor, since the more-oxidized OOA is optically negligible. This weighting assumes the per-source MACs are transferable between sites; because combustion (BBOA/coal) and the less-oxidized secondary factor carry MACs far above the other factors, each site's split is governed by these two mass fractions and is essentially insensitive to the assumed MACs of the weakly-absorbing (more-oxidized secondary and other-primary) factors.

Site (region)	Season	Combustion (BB/coal) (%)	Other primary (%)	Secondary (%)	Reference
This study					
Seoul, Korea	winter	26	6	68	This study
Compiled single-site studies (OA apportionment × this study's MACs)					
Singapore	tropical	0	42	58	Kasthuriarachchi et al. (2020)
Shanghai, China	late spring	0	7	93	Huang et al. (2012)
SE USA (Centreville)	summer, rural	32	0	68	Xu et al. (2015)
Hong Kong	winter	0	9	91	Li et al. (2015)
Barcelona, Spain	winter	35	9	56	Mohr et al. (2012)
Helsinki, Finland	spring	49	5	46	Crippa et al. (2014)
Paris, France	winter	40	7	53	Crippa et al. (2013)
Lanzhou, China	winter	66	5	29	Xu et al. (2016)
Season-matched winter East Asia (directly apportioned, 365 nm)					
Beijing, Harbin, Xi'an — N. China (mean)	winter	n.r.	93	7	Wang et al. (2022)
Chengdu, China	winter	14	65	21	Wang et al. (2022)
Guangzhou, China	winter	0	82	18	Wang et al. (2022)
Wuhan, China	winter	38	43	20	Wang et al. (2022)